In-situ Melt Pool Monitoring of Laser Aided Additive Manufacturing using Infrared Thermal Imaging

L. Chen[1,2], X. Yao[1*], N.P.H. Ng[2], S.K. Moon[2*]

[1]Singapore Institute of Manufacturing Technology, Agency for Science, Technology and Research (A*STAR), Singapore

[2]School of Mechanical and Aerospace Engineering, Nanyang Technological University, Singapore

yao_xiling@simtech.a-star.edu.sg (X. Yao); skmoon@ntu.edu.sg (S.K. Moon)

Abstract - **In-situ monitoring is critical for detecting process anomalies and defect occurrences in additive manufacturing (AM). Traditional vision-based sensing approaches focused on extracting melt pool geometric information, while thermal-based monitoring focused on melt pool temperature measurement. This paper proposes an in-situ melt pool monitoring method utilising infrared thermal imaging for a robot-based direct energy deposition (DED) process. A high-resolution infrared thermal camera is employed to monitor the melt pool region, and a ROS-based multi-nodal software was developed to enable in-situ thermal image processing and melt pool feature extraction. The key contribution of this work is the development of a multi-feature extraction pipeline. Both melt pool geometric and thermal characteristics, such as contour area, centroids, elliptical width, peak temperature, and temperature variance, can be extracted and visualised in real time. The image processing and feature extraction pipeline can work concurrently with the sensor data acquisition. Experiment results are presented to show the effectiveness of the proposed in-situ melt pool monitoring method. It is found that melt pool geometric and thermal features share a similar trend in the temporal domain.**

Keywords - **additive manufacturing; in-situ process monitoring; feature extraction; infrared thermal imaging; melt pool**

I. INTRODUCTION

Additive manufacturing (AM) has grown in popularity in recent years as a result of its distinct advantages in design flexibility, waste reduction, and the ability to fabricate complex geometries [1]. Such benefits are particularly attractive to the aerospace, automotive, and defence industries [2], [3]. However, quality inconsistency and defects remain major problems in most AM processes. In-situ monitoring is the key to detecting process anomalies and enabling adaptive process control to ensure the quality of the as-built products.

Conventional vision-based monitoring techniques focus on the extraction of melt pool geometric characteristics. For example, melt pool geometry captured by a CMOS camera can be correlated to process parameters during the DED process [4], where the melt pool width can directly reflect the laser power level and stability of the process. Based on the melt pool geometric features, adaptive process control can be implemented to reduce process disturbances and enhance the part quality [5].

Vision-based sensing was also used for deposition height monitoring by laser triangulation technique [6]. Recently, the authors' research group proposed a vision-based in-situ monitoring and adaptive process control technique [7]–[10], in which a co-axial CCD camera captures real-time melt pool images, and a laser displacement sensor inspects the in-process part surface conditions. In-situ data processing and machine learning-enabled early surface defect detection can provide feedback that is utilised to adaptively improve the dimensional accuracy.

While vision-based monitoring is useful for understanding the melt pool geometric characteristics, melt pool temperature features and thermal history are also helpful in identifying potential process anomalies and predicting part quality. Recent research on mechanistic property prediction of as-build DED parts based on thermal history has shown great potential [11], [12]. However, in most applications, thermal monitoring was achieved by using a pyrometer sensor [13], or an infrared camera [14], which only obtains temperature readings.

In this paper, we present an in-situ melt pool monitoring method for laser aided additive manufacturing (LAAM) using high-resolution infrared thermal imaging. The real-time thermal images are used to extract multiple melt pool geometric features (e.g., contours, centroids, width, length, etc.) and thermal features (e.g., temperature peak, mean, variance, kurtosis, etc.). A multi-nodal software based on the Robot Operating System (ROS) is developed to support in-situ image processing, feature extraction and visualisation, which operates in parallel and automatically during the LAAM process. The proposed method sets the basis for in-situ quality prediction in AM utilising infrared thermal imaging.

II. METHODOLOGY

A. System setup

As shown in Figure. 1, the proposed in-situ melt pool monitoring system was implemented on a robot-based LAAM cell, which consists of a 6-axis industrial robot (KUKA KR90), a 2-axis positioner, a laser head with a co-axial powder feeding nozzle, and a high-resolution short-wave infrared (SWIR) thermal camera (Infratec). The thermal camera was rigidly mounted on the end-effector of

the robot, which captures melt pool images during the LAAM process with a maximum frame rate of 60 Hz.
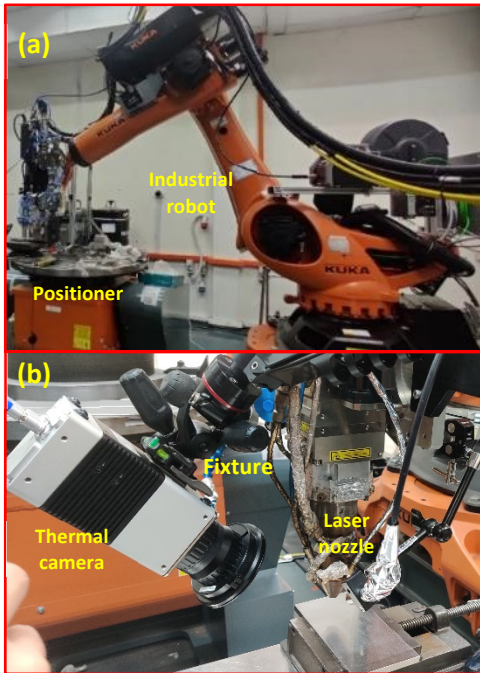
Figure 1. In-situ melt pool monitoring setup: (a) the robot-based LAAM setup, (b) infrared thermal camera mounted beside the laser head with a fixture.

B. ROS-based multimodal software platform

Figure 2 depicts the in-house developed ROS software's Graphical User Interface (GUI) for in-situ monitoring of the LAAM process. The GUI allows for real-time visualisation of raw thermal images, cropped and converted binary melt pool images, and in-situ extracted features. Furthermore, the software platform also supports robot motion monitoring by retrieving the deposition position, velocity, and acceleration from the robot controller via PC-robot ethernet communication.

The details of the software architecture are illustrated in Figure 3. The rectangular blocks denote the "nodes" in ROS programs, and the elliptical blocks represent the "topics" for multi-channel data communication [15]. The infrared thermal camera and robot controller are connected to a PC running the Ubuntu 18.04 operating system. The TCP/IP communication protocol is used by the PC-robot interface. The robot controller transmits data on the robot's joint states (position), velocity, and acceleration to the PC. The PC can also send commands to the sensor and robot, such as switching on the thermal camera and turning on/off the laser. The physical motion of the robot is reflected in the GUI, featuring a digital twin of the real-time LAAM process.

An IR camera driver node acquires raw thermal images via the PC-sensor interface, which is subscribed by the image processing node. Following that, the image processing node performs image thresholding and region

of interest (ROI) extraction. The resultant binarized melt pool region is then utilised to extract geometric features. The melt pool thermal characteristics, on the other hand, are derived straight from the raw images. Both raw and binarized pictures are saved for offline analysis. The "topics" channel's data can be seen in real time in the GUI.

The details on the in-situ geometric and thermal feature extraction are provided in the next section.
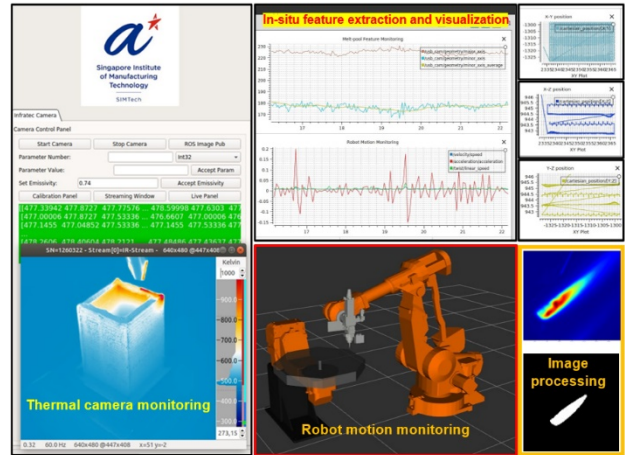
Figure 2. Graphic User Interface (GUI) of the in-house developed ROS software for in-situ process monitoring.
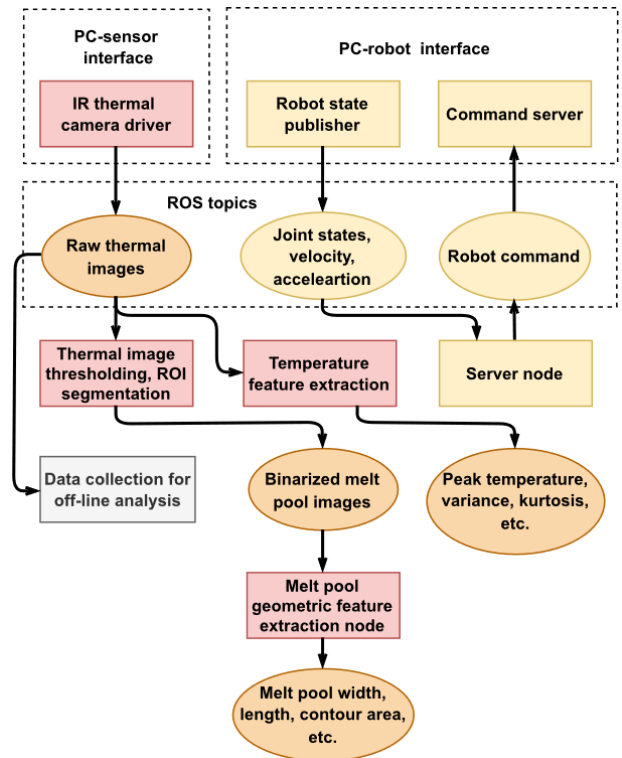
Figure 3. Software architecture

C. In-situ feature extraction

Several key melt pool features are extracted for in-situ monitoring. Table 1 lists the selected melt pool geometric

and thermal features and their mathematical expressions and definitions. Geometric features include melt pool contour area, convex hull area, second moment of area, centroid position, and elliptical width and length. The feature definitions are adapted from [16] and implemented in the OpenCV python library [17]. Apart from geometric features, melt pool thermal features are also extracted. The temperature distribution of the melt pool is related to the process conditions and part quality. Unstable melting states can lead to dimensional inaccuracy, which is attributed to the heating and cooling within the melt pool regions [18]. The melt pool temperature distribution could also reflect the heat transfer conditions. For example, large melt pool temperature variance indicates a strong convection state [18]. Kurtosis is a measure of the non-gaussianity of the melt pool temperature distribution, which is related to deposition speed (i.e., higher speed results in a heavier tail in the molten pool, while lower speed makes the melt pool temperature distribution more gaussian-like). The skewness value quantifies the distribution's asymmetry, which is also affected by the process circumstances. As a result, for thermal feature extraction, the peak temperature, temperature variance, skewness, and kurtosis are chosen.

TABLE I
List of features extracted from the thermal camera

Category	Feature name	Mathematical expression/definitions
Geometric features	Melt pool contour area	$m_{00} = \sum_x \sum_y I(x,y)\Delta A$
	Melt pool second moment of contour area	$x_2 = \dfrac{m_{20}}{m_{00}}; y_2 = \dfrac{m_{02}}{m_{00}}$
	Melt pool centroid position	$\bar{x} = \dfrac{m_{10}}{m_{00}}; \bar{y} = \dfrac{m_{01}}{m_{00}}$
	Convex hull area	Based on OpenCV definition [17]
	Meld pool ellipse width and length	$\dfrac{(x\cos a + y\sin a)^2}{a^2} + \dfrac{(x\sin a - y\cos a)^2}{b^2} = 1$
Temperature features	Peak temperature	Highest temperature value in the current timestamp
	Temperature variance	$Var[X] = S^2 = \dfrac{\sum_i^N (X_i - \bar{X})^2}{(N-1)}$
	Temperature skewness	$\tilde{\mu}_3 = \dfrac{\sum_i^N (X_i - \bar{X})^3}{(N-1)*\sigma^3}$
	Temperature kurtosis	$kurt[X] = E\left[\left(\dfrac{X-\mu}{\sigma}\right)^4\right]$

III. RESULTS AND DISCUSSION

A LAAM experiment was conducted to test the effectiveness of the proposed in-situ melt pool monitoring

method. A rectangular block sample with a 30x30 mm size consisting of 5 layers was deposited using maraging steel 300 powder. The nominal deposition speed was 20 mm/s. The physical positions of robot tool-centre-point (TCP) and velocity data are shown in Figures 4 and 5, respectively. Significant positioning variations and speed inconsistencies are seen during deposition, which might lead to defects in the as-built component.
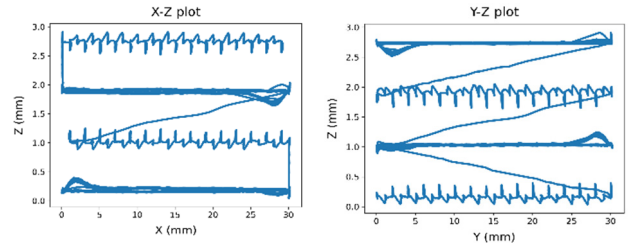
Figure 4. Visualisation of robot TCP position data during the LAAM experiment.
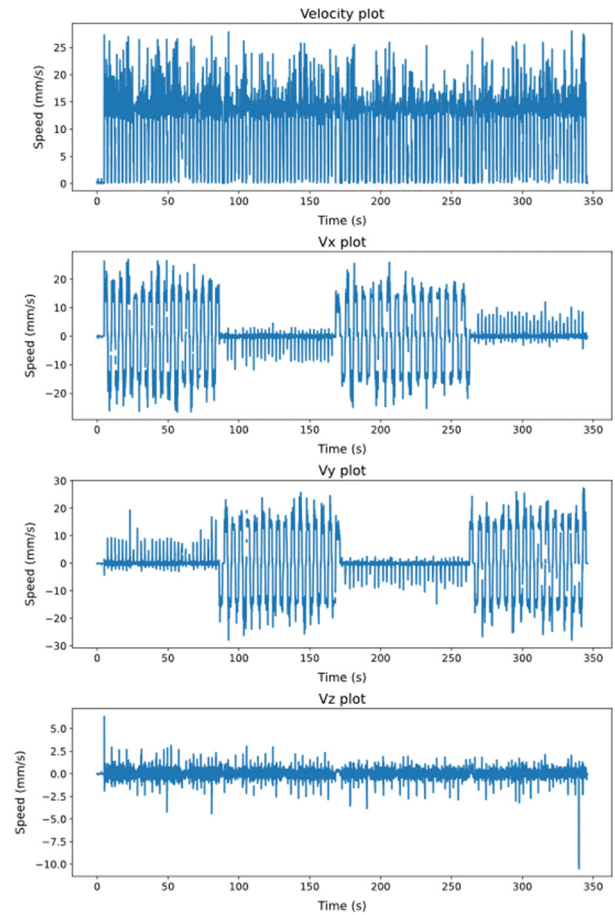
Figure 5. Visualisation of robot TCP velocity data during the LAAM experiment.

The in-situ thermal image processing pipeline for melt pool geometric feature extraction is shown in Figure 6, which was carried out in the ROS node as mentioned in the Section II B. The raw thermal image in RGB colour is shown in Figure 6(a). It was converted into grey scale in

Figure 6(b), with pixel intensities (normalised to 0-255) representing the temperature levels. Figure 6(c) shows the isothermal lines to segment the melt pool area according to the material-specific temperature threshold. The segmented regions are described as the heat affected zone (HAZ), liquid-solid area, and liquid metals, which are key melt pool metallurgical features. Image binarization is conducted on the grey-scale images to isolate the melt pool region of interest (ROI). Based on the binarized images, melt pool contour extraction and elliptical shape fitting is conducted as shown in Figure 6(e) and (f).
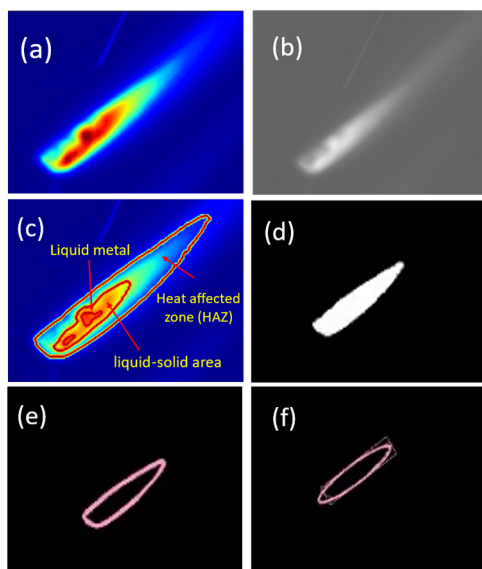
Figure 6．In-situ thermal image processing pipeline: (a) raw thermal image in RGB colour format; (b) grey-scale image with pixel intensities representing temperature levels; (c) melt pool area segmentation by material-specific temperature threshold; (d) binarized melt pool by adaptive thresholding; (e) melt pool contour extraction; (f) melt pool area fitted by elliptical and rectangular shapes.

The extracted melt pool geometric and thermal features were collected during the process for offline analysis. As shown in Figure 7, all the features are normalised so that they have a zero mean and unit variance. It can be observed that all the features share a similar trend. The value in the second layer rises more drastically than in the first, followed by a sharp decline in the third layer. In the fourth layer, the value goes up with much more fluctuations. The variations in the feature might be ascribed to cyclic heating and cooling during deposition, which will be investigated further in the future. In Figure 8, we present a spatial visualisation of the melt pool peak temperature during the LAAM process.
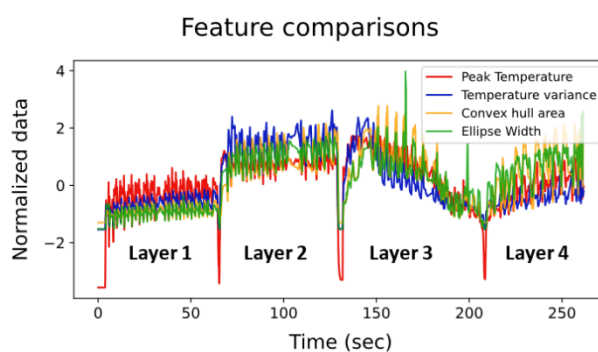
Figure 7. Comparisons of normalised melt pool geometric and thermal features show similar trends.
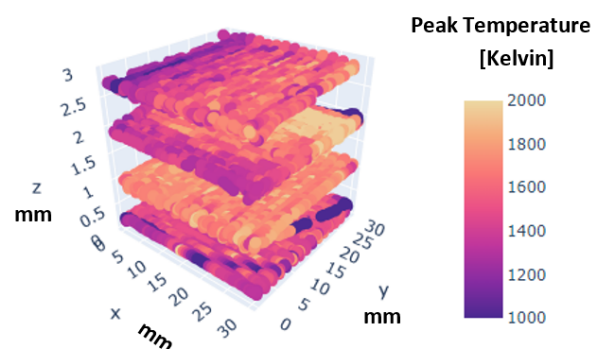
Figure 8. Peak temperature visualised in the spatial domain.

IV. CONCLUSION

In this paper, we presented an in-situ melt pool monitoring approach for the LAAM process based on infrared thermal imaging. The main contribution of this work was to develop a melt pool multi-feature extraction pipeline. During the LAAM process, key melt pool geometric and thermal features were retrieved and visualised in real time. The pipeline for thermal image processing and feature extraction was implemented in an in-house developed ROS software, which allowed for concurrent program execution with shared data communication. The in-situ collected features were visualised and compared. The melt pool's geometric and thermal properties were discovered to have similar tendencies, which would be explored further in our future research.

ACKNOWLEDGMENT

REFERENCES

[1] M. Schmidt, M. Merklein, D. Bourell, D. Dimitrov, T. Hausotte, K. Wegener, L. Overmeyer, F. Vollertsen, and G. N. Levy, "Laser based additive manufacturing in industry and academia," *CIRP Annals*, vol. 66, no. 2, pp. 561–583, Jan. 2017, doi: 10.1016/j.cirp.2017.05.011.

[2] C. Tan, F. Weng, S. Sui, Y. Chew, and G. Bi, "Progress and perspectives in laser additive manufacturing of key aeroengine materials," *International Journal of Machine Tools and Manufacture*, vol. 170, p. 103804, Nov. 2021, doi: 10.1016/j.ijmachtools.2021.103804.

[3] J. C. Vasco, "Additive manufacturing for the automotive industry," in *Additive Manufacturing*, Elsevier, 2021, pp. 505–530. doi: 10.1016/B978-0-12-818411-0.00010-0.

[4] S. Ocylok, E. Alexeev, S. Mann, A. Weisheit, K. Wissenbach, and I. Kelbassa, "Correlations of Melt Pool Geometry and Process Parameters During Laser Metal Deposition by Coaxial Process Monitoring," *Physics Procedia*, vol. 56, pp. 228–238, Jan. 2014, doi: 10.1016/j.phpro.2014.08.167.

[5] B. T. Gibson, Y. K. Bandari, B. S. Richardson, W. C. Henry, E. J. Vetland, T. W. Sundermann, and L. J. Love, "Melt pool size control through multiple closed-loop modalities in laser-wire directed energy deposition of Ti-6Al-4V," *Additive Manufacturing*, vol. 32, p. 100993, Mar. 2020, doi: 10.1016/j.addma.2019.100993.

[6] S. Donadello, M. Motta, A. G. Demir, and B. Previtali, "Monitoring of laser metal deposition height by means of coaxial laser triangulation," *Optics and Lasers in Engineering*, vol. 112, pp. 136–144, Jan. 2019, doi: 10.1016/j.optlaseng.2018.09.012.

[7] L. Chen, X. Yao, P. Xu, S. K. Moon, and G. Bi, "Surface Monitoring for Additive Manufacturing with in-situ Point Cloud Processing," in *2020 6th International Conference on Control, Automation and Robotics (ICCAR)*, Apr. 2020, pp. 196–201. doi: 10.1109/ICCAR49639.2020.9108092.

[8] L. Chen, X. Yao, P. Xu, S. K. Moon, and G. Bi, "Rapid surface defect identification for additive manufacturing with in-situ point cloud processing and machine learning," *Virtual and Physical Prototyping*, vol. 16, no. 1, pp. 50–67, Oct. 2020, doi: 10.1080/17452759.2020.1832695.

[9] P. Xu, X. Yao, L. Chen, C. Zhao, K. Liu, S. K. Moon, and G. Bi, "In-process adaptive dimension correction strategy for laser aided additive manufacturing using laser line scanning," *Journal of Materials Processing Technology*, vol. 303, p. 117544, 2022, doi: 10.1016/j.jmatprotec.2022.117544.

[10] L. Chen, X. Yao, Y. Chew, F. Weng, S. K. Moon, and G. Bi, "Data-Driven Adaptive Control for Laser-Based Additive Manufacturing with Automatic Controller Tuning," *Applied Sciences*, vol. 10, no. 22, Art. no. 22, Jan. 2020, doi: 10.3390/app10227967.

[11] Z. Chen, X. Guo, and J. Shi, "Hardness Prediction and Verification Based on Key Temperature Features During the Directed Energy Deposition Process," *Int. J. of Precis. Eng. and Manuf.-Green Tech.*, Mar. 2020, doi: 10.1007/s40684-020-00208-4.

[12] X. Xie, J. Bennett, S. Saha, Y. Lu, J. Cao, W. K. Liu, and Z. Gan, "Mechanistic data-driven prediction of as-built mechanical properties in metal additive manufacturing," *npj Comput Mater*, vol. 7, no. 1, Art. no. 1, Jun. 2021, doi: 10.1038/s41524-021-00555-z.

[13] G. Bi, B. Schürmann, A. Gasser, K. Wissenbach, and R. Poprawe, "Development and qualification of a novel laser-cladding head with integrated sensors," *International Journal of Machine Tools and Manufacture*, vol. 47, no. 3, pp. 555–561, Mar. 2007, doi: 10.1016/j.ijmachtools.2006.05.010.

[14] Z. Zhang, Z. Liu, and D. Wu, "Prediction of melt pool temperature in directed energy deposition using machine learning," *Additive Manufacturing*, vol. 37, p. 101692, Jan. 2021, doi: 10.1016/j.addma.2020.101692.

[15] M. Quigley, B. Gerkey, K. Conley, J. Faust, T. Foote, J. Leibs, E. Berger, R. Wheeler, and A. Ng, "ROS: an open-source Robot Operating System," p. 6.

[16] C. Knaak, J. von Eßen, M. Kröger, F. Schulze, P. Abels, and A. Gillner, "A Spatio-Temporal Ensemble Deep Learning Architecture for Real-Time Defect Detection during Laser Welding on Low Power Embedded Computing Boards," *Sensors*, vol. 21, no. 12, Art. no. 12, Jan. 2021, doi: 10.3390/s21124205.

[17] G. Bradski, "The OpenCV Library," *Dr. Dobb's Journal of Software Tools*, 2000.

[18] Z. Tang, W. Liu, L. Zhu, Z. Liu, Z. Yan, D. Lin, Z. Zhang, and H.-C. Zhang, "Investigation on coaxial visual characteristics of molten pool in laser-based directed energy deposition of AISI 316L steel," *Journal of Materials Processing Technology*, vol. 290, p. 116996, Apr. 2021, doi: 10.1016/j.jmatprotec.2020.116996.